The novel P_{II}-interacting protein PirA regulates flux into the cyanobacterial ornithine-ammonia cycle

Paul Bolay[a,*], M. Isabel Muro-Pastor[b,*], Rokhsareh Rozbeh[c,*], Stefan Timm[d], Martin Hagemann[d], Francisco J. Florencio[b], Karl Forchhammer[c] and Stephan Klähn[a,#]

[a]*Helmholtz Centre for Environmental Research, Department of Solar Materials, Permoserstr. 15, D-04318 Leipzig, Germany*

[b]*Instituto de Bioquímica Vegetal y Fotosíntesis, CSIC-Universidad de Sevilla, Américo Vespucio 49, E-41092 Sevilla, Spain*

[c]*Interfaculty Institute for Microbiology and Infection Medicine, Organismic Interactions Department, Tübingen University, Auf der Morgenstelle 28, 72076, Tübingen, Germany.*

[d]*Department of Plant Physiology, University of Rostock, Albert-Einstein-Str. 3, D-18059, Rostock, Germany.*

[*]These authors contributed equally.

[#]Address correspondence to stephan.klaehn@ufz.de

Running Head: Regulation of cyanobacterial arginine synthesis

Key words: nitrogen metabolism, cyanobacteria, small inhibitory proteins, P_{II} protein

Abstract (250 words)

Among prokaryotes, cyanobacteria have an exclusive position due to the fact that they perform oxygenic photosynthesis. Cyanobacteria substantially differ from other bacteria in further aspects, e.g. they evolved a plethora of unique regulatory mechanisms to control primary metabolism. This is exemplified by the regulation of glutamine synthetase (GS) via small proteins termed inactivating factors (IFs). Here we reveal another small, 51 amino acid protein, which is encoded by the *ssr0692* gene, to regulate flux into the ornithine-ammonia cycle (OAC), the key hub of cyanobacterial nitrogen stockpiling and remobilization. This regulation is achieved by the interaction with the central carbon/nitrogen control protein P_{II}, which commonly controls the entry into the OAC by activating the key enzyme of arginine synthesis, N-acetyl-L-glutamate kinase (NAGK). We suggest that Ssr0692 competes with NAGK for P_{II} binding and thereby prevents NAGK activation, which in turn lowers arginine synthesis. Accordingly, we termed it **P**$_{II}$-**i**nteracting **r**egulator of **a**rginine synthesis (**PirA**). Similar to the GS IFs, PirA accumulates in response to ammonium upshift due to relief from repression by the global nitrogen-control transcription factor NtcA. Consistently, deletion of PirA affects the cell to balance metabolite pools of the OAC in response to ammonium shocks. Moreover, its interaction with P_{II} requires ADP and is prevented by P_{II} mutations affecting the T-loop conformation, the major protein-interaction surface of this signal processing protein. Thus, we propose that PirA is an integrator determining flux into N storage compounds not only depending on the N availability but also the energy state of the cell.

Importance (150 words)

Cyanobacteria contribute a significant portion to the annual oxygen yield and play important roles in biogeochemical cycles, e.g. as major primary producers. Due to their photosynthetic lifestyle cyanobacteria also arouse interest as hosts for the sustainable production of fuel components and high-value chemicals. However, their broad application as microbial cell factories is hampered by limited knowledge about the regulation of metabolic fluxes in these organisms. Our research identified a novel regulatory protein that controls nitrogen flux, in particular arginine synthesis in the cyanobacterial model strain *Synechocystis* sp. PCC 6803. Beside its role as proteinogenic amino acid, arginine is a precursor for the cyanobacterial storage compound cyanophycin, which is of potential interest to biotechnology. The obtained results will therefore not only enhance our understanding of flux control in these organisms, it will also help to provide a scientific fundament for targeted metabolic engineering and hence the design of photosynthesis-driven biotechnological applications.

Introduction

Nitrogen (N) is one of the key elements of life and needs to be incorporated into biomolecules via assimilatory pathways. Despite an ever-present resource, only a few bacteria can fix dinitrogen (N_2) and the majority of bacteria relies on the uptake and assimilation of combined N sources from their environment (1–3). To respond to fluctuations in the availability of those N sources, bacteria possess complex regulatory networks to control N uptake as well as the activity of assimilatory enzymes (for reviews see (4–7)). As a prime example, glutamine synthetase (GS), a key enzyme of bacterial

ammonium assimilation is tightly regulated in a variety of ways. In *E. coli* and other proteobacteria expression of the GS encoding *glnA* gene is controlled at the transcriptional level by the widespread NtrC/NtrB two-component system (5). Moreover, GS is controlled at the activity level via cumulative feedback inhibition from numerous metabolites related to N and energy metabolism as well as by covalent modification, i.e. adenylylation of the GS subunits. This modification system is operated by a bicyclic modification cascade involving the ubiquitous P_{II} signal transducer protein as regulatory element (reviewed in 8). However, striking differences in comparison to widely accepted paradigms of N assimilation have been revealed in other bacteria, e.g. cyanobacteria.

Cyanobacteria are the only prokaryotes performing oxygenic photosynthesis and play a major role in global biogeochemical cycles (9–11). Nowadays, they receive growing interest as biocatalysts in photo-biotechnological applications, e.g. for the sustainable production of value chemicals and fuels (12–16). To rationally engineer cyanobacteria, i.e. channeling metabolic fluxes to obtain the maximum yield of a desired chemical product, it is of paramount importance to fully comprehend underlying regulatory processes targeting primary metabolism. Albeit our overall understanding of cyanobacterial systems is still fragmentary compared to other well established bacterial models, a few systems have been extensively investigated and include distinctive features. For instance, GS activity is controlled via the interaction with small, inhibitory proteins unique to cyanobacteria (17, 18). These GS inactivating factors (IFs) exclusively control GS activity linearly with their abundance. Moreover, with the global nitrogen control protein NtcA, cyanobacteria use another type of transcription factor to control the expression of genes in response to N fluctuation (19). NtcA belongs to the CRP transcriptional regulator family and commonly works as activator of N assimilatory

genes (20–23). During N-limitation, increasing levels of 2-oxoglutarate and the co-activator protein PipX stimulate DNA binding of NtcA (24–26). The interaction between NtcA and PipX is antagonized by the P_{II} protein, which acts as a global multitasking sensor and regulator, adjusting the carbon-nitrogen homeostasis through versatile protein-protein interactions (27, 28). This, for instance, includes the key enzyme for arginine synthesis, N-acetyl glutamate kinase (NAGK), which is activated by complex formation with P_{II} (29).

In addition to the activation of N assimilatory genes, NtcA can also act as a repressor of genes under N limitation. The physiological consequences of simultaneous positive and negative transcriptional regulation are again exemplified by the well-investigated GS regulatory system. During N-limiting conditions, NtcA activates transcription of the *glnA* gene thereby increasing GS abundance and the rate of ammonium assimilation. Simultaneously, enhanced DNA binding of NtcA represses transcription of the genes *gifA* and *gifB* encoding the two known IFs, IF7 and IF17 (30). Thereby, GS activity is tuned in a tradeoff between cellular N demands and relief from the metabolic burden imposed by the glutamate and ATP-consuming GS catalyzed reaction (for a review see 30). Besides *gifA* and *gifB*, only a few other genes appear to be negatively regulated by NtcA. In an attempt to define the entire regulon of NtcA in the unicellular model strain *Synechocystis* sp. PCC 6803 (hereafter *Synechocystis*), Giner-Lamia et al. identified the gene *ssr0692* as another NtcA-repressed candidate (20). It encodes a small protein consisting of 51 amino acids with a high portion of N-rich, positively charged residues, which were shown to be indispensable for protein-protein interaction in case of the GS IFs (18). These distinguishing traits point towards a vital function related to N control similar to the known GS IFs, e.g. as a regulator of a metabolic pathway.

Here we report on the functional analysis of the small protein Ssr0692 in *Synechocystis*. It accumulates in response to ammonium supply and fulfills crucial regulatory roles in cyanobacterial metabolism via the interaction with the P_{II} signaling protein. We suggest that it interferes with the P_{II}-dependent activation of NAGK. Consistently, under fluctuating N regimes *ssr0692* mutant strains are impaired in balancing synthesis of arginine and other amino acids associated with the cyanobacterial ornithine ammonia cycle identified recently (32). We therefore named Ssr0692 as **P**$_{II}$-**i**nteracting **r**egulator of **a**rginine synthesis (**PirA**).

Results

Homologs of the *pirA* gene of *Synechocystis* are frequently present in cyanobacterial genomes and show a high degree of sequence conservation at the amino acid level (**Fig. 1A,B**). With only a few exceptions sequences similar to PirA are absent from genomes of other bacterial phyla (as of July 2020 exceptions are: *Candidatus Gracilibacteria bacterium, Chloroflexaceae bacterium, Flavobacterium sp.* CLA17*, Methylacidiphilales bacterium*). At first glance, this observation suggests a function associated with oxygenic photosynthesis. However, *pirA* has previously been identified as part of the NtcA regulon in *Synechocystis* (20) consistent with two putative NtcA binding motifs located upstream of the transcriptional start site (TSS) (**Fig. 1C**). In promoters that are activated by NtcA, the respective binding motifs are centered close to position -41.5 with regard to the TSS bringing NtcA into a favorable position to promote the binding of RNA polymerase (33). However, the distal motif upstream of *pirA* centers at -48.5, which contradicts the typical position in NtcA-activated promoters. Moreover, the proximal motif centers at -33.5 bp upstream of the TSS, i.e. the first nucleotide is located at position -40 (**Fig. 1C**). This resembles the situation upstream of the *gifA/B* genes, which are also negatively regulated by NtcA (20). Both

genes harbor binding motifs that are situated in close proximity or even directly adjacent to the TSS (30), thereby blocking the access of RNA-polymerase. Accordingly, the motif location upstream of *pirA* indicates a negative regulation by NtcA. This assumption is consistent with its downregulation under N limitation, similar to the *gifA/B* genes and in contrast to NtcA-activated genes such as *glnA* or *nrtA* encoding GS and a nitrate transporter component, respectively (**Fig 1D**).

PirA accumulates under N excess and is linked to a function in cyanobacterial N metabolism

Genes that are repressed by NtcA, such as the *gifA/B* genes, show low or even non-detectable transcription under N limitation but are highly expressed in response to excess N supply. To test whether this is also true for *pirA*, we pre-cultivated *Synechocystis* cells in presence of nitrate and analyzed transcript levels after induction of N excess by adding 10 mM ammonium. As expected, the *pirA* mRNA strongly accumulated under these conditions (**Fig. 1E**). To investigate whether this regulatory pattern is conveyed to the protein level, we obtained an antibody specific to the PirA protein. Consistent with the observed transcriptional regulation, the PirA protein also accumulated in response to ammonium upshifts (**Fig. 1F**). Moreover, the protein appeared to have a high turnover due to the fact that it eluded detection shortly after N was depleted. These observations clearly link PirA and its function to cyanobacterial N metabolism.

To investigate the biological function of PirA, knockout and overexpression strains for the *pirA* gene were established in *Synechocystis*. The knockout mutant Δ0692 was generated by replacing the entire *pirA* open reading frame with a kanamycin resistance cassette via homologous recombination. In case of the overexpression strain 0692^{+}, a pVZ322 plasmid derivative harboring a transcriptional fusion of *pirA* with the Cu^{2+}-

inducible *petE* promoter was transferred into *Synechocystis* WT (for a schematic overview of the constructs see **Fig. 2A**). Full segregation of the mutant allele in Δ0692 as well as the presence of the recombinant plasmid in 0692^{+} were verified by PCR (**Fig. 2B**). Subsequent Northern-blots with RNA isolated from cells grown in presence of 1 µM $CuSO_4$ confirmed the generated mutants: the overexpression strain showed increased *pirA* mRNA levels compared to WT while in the knockout strain the *pirA* transcript was absent (**Fig. 2C**). Interestingly, even though the mRNA was present and its abundance significantly increased in strain 0692^{+} due to the ectopic expression triggered by Cu^{2+}, the PirA protein could not be detected in nitrate-grown cells. However, after adding ammonium, which triggers expression of the native *pirA* gene from the chromosome, increased PirA levels were detectable in strain 0692^{+} compared to the WT (**Fig. 2D**). This, in addition to the confirmed increase at the mRNA level, clearly confirmed that the overexpression construct is operative. Obviously, PirA abundance is not exclusively controlled at the transcriptional level. This observation was further supported by experiments using a *pirA* knockout mutant in which a P*petE*-fused gene copy was introduced. As observed before, the PirA protein could not be detected after adding Cu^{2+} to nitrate-grown cells (**Fig. 2E**). Remarkably, its presence was still N-dependent similar to WT, i.e. it was detectable only after adding ammonium (**Fig. 2E**) even though *pirA* transcription was controlled by P*petE* and hence, exclusively triggered by Cu^{2+}. Consequently, these data indicate an additional, posttranscriptional control mechanism, which obviously prevents stable PirA accumulation unless N availability suddenly increases. This again resembles the GS IFs encoded by the *gifA/B* genes, which are tightly regulated at the transcriptional as well as posttranscriptional level (34–36).

PirA plays a critical role upon changes in the C/N balance

Under standard conditions, i.e. with nitrate as sole N source and under ambient CO_2, at which PirA is not detectable in WT, the *pirA*-manipulated recombinant strains grew similarly to WT as expected (**Fig. 3A,C**). Given the fact that PirA rapidly accumulated in response to an increasing N availability, which suggests a function related to these conditions, it was tempting to speculate whether both recombinant strains show a phenotype, e.g. an affected pigment synthesis/degradation when the N concentration is altered. In order to test this, we cultivated the WT, Δ0692 and 0692^+ under N oscillating conditions. For that, we inoculated cultures in nitrate-free BG11 and cultivated for three days, which was accompanied by pigment degradation (**Fig. 3B,C**), causing nitrogen-starvation induced chlorosis (37). Cultures of both recombinant strains showed the same behavior as the WT and did not show a non-bleaching phenotype as for instance known for *nbl* mutants that are affected in phycobilisome degradation (38). Consistently, the phycocyanin content was strongly reduced in all cells, measured by the diminished absorption at 630 nm (**Fig 3D**, Day 3). The similar bleaching kinetics of all strains is consistent with the fact that PirA is not detectable under N limitation. Afterwards, the fully chlorotic cells were exposed to consecutive pulses of limited amounts of ammonium (1 mM) to simulate conditions at which PirA is rapidly accumulating and likely important. The re-greening process was monitored by measuring growth as well as whole cell absorption spectra at wavelengths in the range between 400 and 750 nm. While growth recovery was rather similar in all three strains, a clearly altered pigmentation was observed in strain 0692^+ after these ammonium pulses (**Fig. 3C, D**). Consistent with the visible difference, a lower absorption at 630 nm was detected resulting from a reduced phycocyanin content. These data indicate that the cells are impeded in coping with fluctuating N concentrations and struggle to recover from chlorosis when PirA accumulation is not correctly balanced. This supports

the assumption that this small protein plays a crucial role and might participate in regulatory processes that control N metabolism.

Altered PirA abundance affects metabolites of N metabolism

To further examine a potentially regulatory function of PirA, time-resolved quantification of selected metabolites was performed for nitrate-grown cells of the WT and both mutants after addition of 10 mM ammonium. Interestingly, perturbation of PirA levels had a distinctive impact on the accumulation of several key metabolites in *Synechocystis*. Most intriguingly, kinetics of metabolites that are part of or are associated with the recently discovered ornithine-ammonia cycle (32) were strongly affected in strains Δ0692 and 0692^{+} compared to the WT (**Fig. 4**). In general, N upshift triggered a transient accumulation of citrulline, ornithine as well as arginine and aspartate in WT cells similar to previous reports (32). Interestingly, absence of PirA intensified and prolonged the accumulation of these metabolites while overexpression of *pirA* prevented or delayed their accumulation to a significant extend (**Fig. 4**). Moreover, kinetics of glutamine and glutamate, both key amino acids in N metabolism, showed striking differences between the tested strains. For instance, glutamate, which represents the main N-donor in a plethora of pathways was significantly decreased in strain 0692^{+} throughout the experiment. The data clearly indicate that PirA plays a pivotal role in balancing fluxes through or into key amino acids such as arginine. In cyanobacteria, the rate-limiting step of arginine synthesis is controlled by a well-investigated regulatory mechanism, through complex formation of the key enzyme NAGK with the P_{II} protein (28, 29, 39). Moreover, a PII variant with highly increased affinity towards NAGK (PII-I86N) causes constitutive NAGK activation and hence arginine accumulation (40), which was also observed in our study in cells of Δ0692. It was thus tempting to speculate if PirA might interfere at this regulatory node.

PirA interacts with the signaling protein P_{II} in an ADP-dependent manner

Recently, PirA was found enriched in pull down-experiments of the signaling protein P_{II} (41). This indicated that PirA may directly interact with the P_{II} protein and thereby exercise a regulatory function similar to other small P_{II} interacting proteins such as PipX (24) or CfrA/PirC that has recently been discovered by two independent laboratories (42, 43). To verify the interaction between PirA and P_{II} from *Synechocystis*, *in vitro* binding experiments were performed using Bio-layer interferometry (BLI). To this end, recombinant protein variants were expressed in and purified from *E. coli*. His_6-tagged P_{II} protein was immobilized on a Ni-NTA coated sensor tip and a GST-tagged PirA variant was used as analyte in presence or absence of various effector molecules (**Fig. 5A**). Indeed, complex formation was detected in presence of ADP in a clear concentration dependent manner (**Fig. 5B**). In contrast, no interaction was observed in presence of ATP, mixtures of ATP and 2-OG or when no effector molecule was present. These data unambiguously revealed ADP-dependent interaction between P_{II} and GST-tagged PirA. To test the specificity of the interaction, we performed similar measurements using PirA variants, where the GST-tag was removed by proteolytic cleavage. The small PirA peptide yielded a binding signal that was about six-fold lower than the signal observed for the GST fusion protein (**Fig. 5C**). This agrees well with the expected signal, since the BLI-response depends on the mass changes at the sensor tip (GST-PirA vs. PirA: 31.8 kDa/5.8 kDa = 5.5). Furthermore, providing only the GST-tag (26 kDa) did not result in any detectable signal (**Fig. 5C**), which clearly confirms that P_{II} specifically interacts with PirA in these binding experiments. Since the GST-fusion protein is more accurately to handle and the signal is superior to the isolated PirA peptide, further experiments were performed with GST-tagged PirA.

To further study the P_{II}-PirA interaction, different P_{II} variants were examined. In most cases, interaction of proteins with P_{II} involves the highly flexible T-loop structure that can adopt a multitude of conformations (27, 44). Accordingly, a P_{II} variant lacking the T-loop ($P_{II}(\Delta T)$-His_8) was also tested. As expected, no response was observed confirming interaction with PirA via the T-loop (not shown). Moreover, we tested the variant P_{II}(I86N), where a single amino acid replacement, Ile86 to Asp86, locks the T-loop in a conformation that promotes constitutive NAGK binding (45, 46). Strikingly, this variant was not able to bind PirA even in presence of 2 mM ADP that otherwise promotes binding to the native P_{II} (**Fig. 5D**). In contrast, the phosphomimetic variant P_{II}(S49E), which does not interact with NAGK (47), shows unaffected complex formation with PirA (**Fig. 5D**). Affinity of P_{II}(S49E) to PirA was even slightly higher than observed for the native variant (K_D values: 2.9 ± 0.34 µM P_{II}(WT); 2.5 ± 0.27 µM for P_{II}(S49E). Obviously, a conformation of the T-loop that mediates a high P_{II} affinity to NAGK prevents its interaction with PirA. Together with the metabolite profiles showing dysregulated arginine synthesis in the Δ*pirA* mutant, the present data implicate interference of PirA with NAGK regulation through interaction with P_{II}.

Discussion

Arginine serves as proteinogenic amino acid and precursor for the synthesis of polyamines and other N storage compounds such as the cyanobacterial cyanophycin. In bacteria arginine is synthesized either by a linear pathway, e.g. present in *Enterobacteriaceae*, or an energetically more favorable cyclic pathway, where N-acetyl-ornithine reacts with glutamate to yield ornithine and N-acetyl-glutamate, the starting metabolite of the pathway. The latter pathway is widely distributed in nature and also present in cyanobacteria (48, 49). Nevertheless, arginine synthesis requires vast amounts of energy and nitrogen (39) and is thus tightly regulated in bacteria. This

is mainly achieved by feedback inhibition of the corresponding key enzymes by the end product arginine. In *E. coli,* this addresses N-acetylglutamate synthase (NAGS), which catalyzes the first step of linear arginine synthesis from glutamate (48). By contrast, in those bacteria harboring the cyclic pathway, the second enzyme NAGK is feedback inhibited by arginine (49).

A novel player in the distinctive regulation of arginine synthesis in cyanobacteria

In cyanobacteria NAGK is target of a molecular regulatory mechanism that involves complex formation with the signal transduction protein P_{II} (29, 47). This interaction diminishes feedback inhibition of NAGK by arginine and, hence, boosts the metabolic flux towards the end product (29). Its importance for the control of cyanobacterial metabolism is supported by the fact that this mechanism is widely present in oxygenic phototrophs such as plants (50, 51) and microalgae (52) but appears to be absent from other bacteria (for an overview see (53). Regarding arginine metabolism the uniqueness of cyanobacteria within the prokaryotes is also exemplified by the recent discovery of active cycling between ornithine and arginine via an ornithine-ammonia cycle (OAC), similar to the known ornithine-urea cycle (OUC) that is present in terrestrial animals but typically absent from bacteria (32).

Here we propose the small cyanobacterial protein PirA as a novel key regulator in the cyanobacterial arginine synthesis pathway and, hence, also the OAC. Our data confirm PirA accumulation under N excess, in particular when ammonium is added. This accumulation is obviously required to adjust a certain pool of metabolites that are part of the OAC, including arginine. Mechanistically, we propose a model where PirA competes with NAGK for the P_{II} protein (**Fig. 6**). In response to ammonium addition, the high levels of PirA accumulation interfere with complex formation between P_{II} and

NAGK, thereby mitigating the activation of NAGK and preventing an over-accumulation of arginine. Surprisingly, detectable PirA accumulation only occurred under ammonium shock, even when *pirA* mRNA was transcribed independently from N and energy status of the cell. A similar situation can be encountered with the GS IFs, which were shown to be degraded by metalloproteases when not bound to GS (34). Thus, it is tempting to speculate that PirA accumulation can only occur when bound to PII.

PirA integrates N- and energy sensing

Remarkably, PirA only forms a complex with P_{II} in the presence of ADP. Accordingly, the pivotal stimulus for the suggested regulatory mechanism is not only the N status, which is mainly sensed by 2-OG in cyanobacteria similar to other prokaryotes (54, 55). The 2-OG level determines the affinity of NtcA to its binding motif (21, 26), which therefore also determines PirA accumulation. Moreover, PirA was found to transiently but strongly accumulate during low C supply (56). This is consistent with the de-repression of the *pirA* gene by the dissociation of NtcA from its binding motif upstream since low C supply, i.e. a low C/N ratio leads to a decreased 2-OG pool (57). The interaction between PirA and P_{II} strongly responds to ADP as another signal and hence, also depends on the cellular energy status. These observations resemble another small P_{II}-interacting protein, PipX, whose interaction with P_{II} is enhanced by ADP as well (58, 59). PipX functions as co-activator of the transcription factor NtcA and is required for the 2-OG-dependent DNA binding and transcriptional activation of genes (24). In presence of high ADP levels, PipX preferably interacts with P_{II}, which attenuates NtcA activity and in turn leads to de-repression and upregulation of the *pirA* gene, similar to the *gif* genes encoding the GS IFs (30).

Interestingly, *in vitro* data showed that the NAGK-P_{II} interaction is also ADP-sensitive. While ADP does not entirely prevent complex formation, it increases dissociation of

343 NAGK from ADP-bound P_{II} (45). However, detailed analysis of NAGK-P_{II} complex
344 formation demonstrated that this interaction is mainly tuned by 2-OG and not the
345 energy status of the cell (58, 60). It should be kept in mind that the sensing properties
346 of P_{II} are influenced by the binding partner in such a way, that for certain targets, small
347 fluctuation in the ADP/ATP rations are sensed (e.g. P_{II}-PipX complex formation)
348 whereas in other cases, fluctuation in the 2-OG levels are perceived (e.g. P_{II}-NAGK
349 interaction). In light of these data, PirA appears to amplify the energy-dependent signal
350 in P_{II}-mediated activation of NAGK: by sequestering P_{II} under conditions of low 2-OG
351 and high ADP-levels, PirA may shift the equilibrium of P_{II}-NAGK complex towards non-
352 complexed NAGK when the cell experiences energy limitation due to high GS activity
353 in consequence of ammonium addition.

354 Depending on the detailed structure of the complexes, P_{II} phosphorylation either
355 abrogates interaction with its targets, as demonstrated for NAGK (29), or has no effect
356 on them, as in the case of PII-PipX interaction (33). The phosphomimetic variant
357 P_{II}(S49E) showed slightly enhanced interaction with PirA as compared to P_{II}(WT). In a
358 similar way, P_{II} interacts with PipX irrespective of Ser49 modification, but nevertheless,
359 the interaction is T-loop dependent (24). The major interaction surface is at the
360 proximal part of the T-loop, whereas the tip region with the critical Ser49 residue does
361 not participate in complex formation. From the Ser49-independent mode of PirA-P_{II}
362 interaction it can be concluded that the PirA-P_{II} interaction could also take place with
363 phosphorylated P_{II} that does not bind to NAGK. In any case, the interaction of P_{II} with
364 NAGK or PirA appears to be mutually exclusive since both PII-interaction partners
365 require the T-loop in different conformation for interaction. The competition between
366 NAGK and PirA for P_{II} is further illustrated by the inability of PirA to bind P_{II}(I86N). This
367 variant adopts a constitutive NAGK-bound like structure of the T-loop (45, 46).

Accordingly, the lack of interaction with P_{II}(I86N) also agrees with the strong *in vivo* activation of NAGK by this variant (40). However, for a more detailed understanding of the mechanism, by which PirA affects P_{II} signaling, functional biochemical studies and structural analyses are required.

Further implications of PirA beyond arginine synthesis

PirA potentially fulfills several other functions since it appears to feature additional interaction partners, as suggested by previous high-throughput yeast-two hybrid analyses. Among them are NADH dehydrogenase subunit NdhH, DNA polymerase I PolA, the ATP-dependent helicase PcrA as well as several unknown and hypothetical proteins (61). Moreover, *pirA* overexpression was shown to significantly improve butanol tolerance in *Synechocystis* (62). As solvents like butanol compromise cell membrane integrity resulting in loss of proton motive force, the cell increasingly accumulates reactive oxygen species (ROS) through enhanced respiration in an attempt to catch up on lost ATP (63, 64). Given that PirA appears to protect adenylate energy pools, an interaction with players involved in processes that consume large quantities of nucleotides, e.g. DNA replication, appears meaningful. Moreover, overexpression of PirA might result in reduced ROS production as the cell retains sufficient amounts of ATP.

The occurrence of PirA homologs in other cyanobacterial strains does not coincide with a certain lifestyle or phylogeny. For instance, the *pir*A-homolog *asr1328* of the filamentous, diazotrophic cyanobacterium *Anabaena* sp. PCC 7120 was shown to be negatively regulated by NtcA as well (65). Similar to the GS IFs, gene annotations in a few strains such as *Thermosynechococcus elongatus* or *Synechococcus sp.* JA-3-3Ab suggest that alternative versions of PirA with an extended N-terminus might also exist (**Supplementary Fig. S1**). Nevertheless, the existence of those proteins has not been

393 experimentally shown yet, and hence, false annotations cannot be excluded. This
394 assumption is supported by the fact that on the one hand only a few of those elongated
395 sequences could be found in protein databases, which on the other hand only show
396 partial similarity. Therefore, the function of these N-terminal extensions remains
397 elusive to date. In addition, it is worth noting that PirA is, similar to the GS IFs,
398 completely absent in marine picocyanobacteria (**Fig. 1**). In accordance, these clades
399 lack several salient features of N-sensing and utilization which are widespread among
400 cyanobacteria. For instance, P_{II} is not subject to phosphorylation in *Prochlorococcus*
401 (66, 67), and both *Prochlorococcus* and *Synechococcus* genera are incapable of
402 cyanophycin synthesis and lack several OAC cycle genes (68). These genome-
403 streamlined strains occur in oligotrophic realms of the ocean with hardly any fluctuation
404 in nutrient supply (69). Thus, it is compelling to speculate that PirA-mediated short-
405 term adjustment of arginine synthesis to the N and energy status of the cell is not
406 required in such habitats.

407

408 ## Material & Methods

409 ### Strains and growth conditions

410 A *Synechocystis* sp. PCC 6803 strain originally obtained from N. Murata (Japan) was
411 used as wild type. Cells were grown in BG11 medium (70) depleted in Cu^{2+} ions and
412 supplemented with 10 mM TES buffered at pH 8.0. The sole N source in that medium
413 is nitrate at a concentration of 17.64 mM (stated as nitrate-grown). Cultivation was
414 performed in buffled Erlenmeyer flasks in presence of ambient CO_2 under constant
415 illumination (white light, 50µE), at 30°C, 75% humidity and 150 rpm. Each recombinant
416 strain was isolated on BG11-agar plates and maintained in medium containing either

kanamycin or gentamycin at a concentration of 50 µg/ml and 2 µg/ml, respectively. Prior to the experiments investigating the impact of altered PirA abundance the cultures were supplemented with 1 µM $CuSO_4$.

Mutant strain generation

To knockout the *ssr0692* (*pirA*) gene, the upstream and downstream region of *pirA* were amplified from *Synechocystis* gDNA using primer combinations Ssr0692upst_fw/Ssr0692upst_rev and Ssr0692downst_fw/Ssr0692downst_rev, respectively (all primers are listed in **Supplementary Table S1**). The kanamycin resistance cassette was amplified from a customized construct obtained by gene synthesis using primers KmR_fw and KmR_rev. The synthesized construct harboured the *aphII* gene and its promoter which were originally obtained from pUC4K (Amersham). In addition, an *oop* terminator was introduced downstream of *aphII*. All amplicons had short fragments of sequence complementarity and were fused via polymerase cycling assembly (PCA) using primers Ssr0692upst_fw/ Ssr0692downst_rev. The resulting construct was introduced into pJET1.2 (Thermo Scientific) and used to transform chemically competent *E. coli* DH5α. After isolation of the pJET_ssr0692_KmR_KO plasmid from *E. coli*, the knockout construct was introduced into *Synechocystis* WT by natural transformation and homologous recombination into the chromosome. To enable overexpression of *pirA*, the 5' UTR and 3'UTR of the *petE* gene were amplified from *Synechocystis* gDNA using primers PpetE_fw(XhoI)/5'petE_ssr0692_rev and 3'petE_ssr0692_fw/Toop_rev(AseI). The *pirA* coding sequence was amplified from *Synechocystis* gDNA using primers ssr0692_fw/rev. All amplicons were fused via PCR and introduced into the broad-host range plasmid pVZ322 via restriction digestion and ligation into XhoI/AseI sites. The recombinant plasmid pVZ322-PpetE:*ssr0692,* obtained after transformation of and

purification from *E. coli* DH5α, was introduced into *Synechocystis* WT via electroporation. All strains and constructs were verified by PCR and Sanger sequencing.

To generate the alternative Δ0692/P_{petE}-ssr0692 strain (chromosomal integration) a DNA fragment containing *ssr0692* gene including the sequence coding for six histidine residues was amplified by PCR using genomic DNA and primers ssr0692.KpnI and ssr0692.HisBamHI. This fragment was cloned into *Kpn*I-*BamH*I digested pPLAT plasmid(34), a pGEM-T derivative containing a 2 kb region of the non-essential *nrsBACD* operon (71). The *petE* promoter was amplified by PCR using genomic DNA and primers P*petE*.KpnI.1 and P*petE*.KpnI.2 and cloned into *Kpn*I site of *ssr0692*-containing pPLAT. Finally, a Km^r CK1 cassette from pRL161 (72) was cloned in the *BamH*I site of pPLAT, generating pPLAT-P*petE*.ssr0692. This plasmid was used to transform the Δ0692 strain. All generated strains and their properties are given in **Supplementary Table S2**.

N-oscillation experiment

Wild type and mutant strains where inoculated in triplicates at OD_{750} = 0.1 in 3-buffled 100 ml flasks in 20 ml N-depleted BG11 supplemented with 1µM $CuSO_4$. For comparison, the same strains were also cultivated in standard BG11 medium containing 17.64 mM nitrate. After 3 days, the N-starved cells where supplemented with 1mM NH_4Cl, a step which was repeated after 5 and 6 days. Whole cell spectra of cell suspensions were conducted with a Cary 300 UV/Vis Spectrophotometer (Agilent).

RNA extraction and Northern blots

Cells for northern blot analysis were harvested by rapid filtration on polyether sulfone filters (pore size 0.8 µm, PALL). Filters were immediately resolved in 1 ml PGTX solution (73) and frozen in liquid N_2. RNA extraction was conducted as previously

described (74). For northern blots, 3 µg of RNA were separated on MEN-buffered 1.5% agarose gels that provided denaturing conditions by 6% formaldehyde using an RNA sample loading buffer containing a final concentration of 62.5% (v/v) deionized formamide (Sigma-Aldrich). Afterwards, RNA was transferred via capillary blotting to an Amersham Hybond N^+ nylon membrane (GE healtcare) and cross-linked with 1250 µJ in a UVP crosslinker (Analytik Jena). To specifically detect the *pirA* transcript, the RNA-mounted nylon membrane was hybridized with a complementary, α-^{32}P-labeled ssRNA probe that was generated by *in vitro* transcription using the MAXIscript® T7 Transcription Kit (Thermo Fisher Scientific). As transcription template a DNA fragment obtained by PCR with primers Ssr0692_T7_fw and Ssr0692_rev was used. Subsequently, Fuji BAS-IIIS imaging plates were exposed to the membranes and read out by an Amersham Typhoon laser scanner (GE Healthcare). As loading control, the same membranes were hybridized with ssRNA probes complementary to the 5S rRNA, which were generated in the same way using primers 5sRNA_fw/rev (**Supplementary Table S1**).

Anti-PirA antibody production

A DNA fragment encompassing the *pirA* ORF was amplified by PCR from *Synechocystis* genomic DNA, using the oligonucleotides Ssr0692ORF-fw and Ssr0692ORF-rv. This fragment was cloned into pET24a(+) plasmid *NdeI-Xho*I digested (Novagen) to generate pET24-Ssr0692 plasmid. Exponentially growing *E. coli* BL21 cells transformed with pET24-Ssr0692 were treated with 1 mM of isopropyl ß-D-1-thiogalactopyranoside for 4 h. For purification of PirA-His_6 protein, cells were collected, resuspended in buffer A (20 mM sodium phosphate, pH 7.5, 150 mM NaCl, 5 mM imidazole) with 1 mM phenylmethylsulfonyl fluoride (PMSF) and disrupted by sonication. The lysate was centrifuged at 18.000 x *g* for 20 min. PirA-His_6 from the

supernatant was purified by Ni-affinity chromatography using HisTrapHP column (GE Healthcare) and following the manufacturer's instructions. Elution was performed with a linear gradient (5-500 mM imidazole) in buffer A. Fractions with PirA-His_6 were pooled, concentrated using Centrifugal Filter Units (Amicon Ultra-15 3 kDa) (Millipore), and subjected to gel filtration chromatography using a Hiload 16/60 Superdex 75 gel filtration column (GE Healthcare) running on an AKTA FPLC system. Fractions containing purified PirA-His_6 protein were pooled, concentrated and quantified in a NanoDrop 1000 spectrophotometer (Thermo scientific) using the extinction coefficient of PirA-His_6 calculated with ExPASy-ProtParam tool. Anti-PirA antiserum was obtained according to standard immunization protocols by injecting 1.5 mg of purified PirA-His_6 protein in rabbits.

Preparation of crude extracts and Western blot analysis

For the analysis of proteins abundance, 2 U OD_{750} were harvested and resuspended in 80 µl of 50 mM HEPES-NaOH buffer (pH 7.0), 50 mM KCl, 1 mM phenylmethylsulfonyl fluoride (PMSF). Crude extracts were prepared using glass beads as previously described (75). For western blot analysis, proteins were fractionated on 15% SDS-PAGE (76) and transferred to nitrocellulose membranes (Bio-Rad). Blots were blocked with 5% (w/v) non-fat dry milk (AppliChem) in PBS-Tween 20. Antisera were used at the following dilutions: Anti-PirA (1:5000) and anti-TrxA (1:10000)(77). The ECL Prime Western Blotting Detection Reagent (GE Healthcare) was used to detect the different antigens with anti-rabbit secondary antibodies (1:25000) (Sigma-Aldrich).

Metabolite analysis

For metabolite analysis, cells were grown in BG11 containing the standard nitrate amount until reaching OD_{750} ~0.8. Cells were harvested shortly before and after the

addition of 10 mM ammonium chloride by centrifugation of 2 ml culture at 17,000 x *g* for 1 minute. Supernatant was discarded and pellets were snap frozen in liquid N. Metabolite extraction was performed by resuspending cell pellets in 1 ml of 80% [v/v] ethanol supplemented with 1 µg/ml L-carnitine hydrochloride as internal standard and heating for 2 h at 60°C. After centrifugation at 17,000 x *g* for 5 minutes, the supernatant was transferred to a fresh vial and the pellet was again resuspended in 1 ml of 80% [v/v] ethanol and heated at 60°C for 2h. After centrifugation at 17,000 x *g* for 5 minutes, supernatants were combined and dried in a centrifugal evaporator.

Next, the dried extracts were dissolved in 1000 µL LC-MS grade water and filtrated through 0.2 µm filters (Omnifix-F, Braun, Germany). 1 µl of the cleared supernatants were analyzed using the high-performance liquid chromatograph mass spectrometer LCMS-8050 system (Shimadzu) and the incorporated LC-MS/MS method package for primary metabolites (version 2, Shimadzu) as described in (78).

Bio-layer interferometry (BLI)

Protein interaction studies via Bio-layer interferometry (BLI) were performed on an Octet K2 instrument (Fortébio Molecular Devices (UK) Limited, Wokingham, United Kingdom), which allows simultaneous binding experiments on two channels, one of which is used as negative control. All experiments were done in buffer containing 50 mM Tris-HCl pH 7.4, 150 mM KCl, 2 mM $MgCl_2$, 0.02% LDAO and 0.2mg/ml BSA. Effector molecules were used at following concentrations: 2 mM ATP, 2 mM 2-OG and 0.1, 0.25, 0.5, 1 and 2 mM for ADP. Interaction experiments were performed as reported previously (43). Briefly, His_8-tagged variants of P_{II}, namely P_{II}(WT), P_{II}(S49E), P_{II}(I86N) and P_{II}(ΔT)-His_8 were used as ligands bound to Ni-NTA coated sensor tips. Various concentrations of GST-PirA from 125 to 12000 nM were used as analyte to display association reactions at 30˚C. As preliminary experiments showed GST-PirA

542 binds unspecifically to the Ni-NTA sensor tips, the non-interacting $P_{II}(\Delta T)$ variant was
543 used to saturate the tips and thereby remove unspecific binding. The binding of P_{II}
544 ligands was performed by first loading 10 µg/ml of P_{II} on the Ni-NTA sensor tip, followed
545 by dipping the tip into buffer for 60 s (to remove unbound P_{II}) and recording the first
546 baseline. To block unoccupied sites on the sensor surface, that cause disturbing
547 unspecific binding, 72 µg/ml $P_{II}(\Delta T)$ was loaded onto the tip. Afterwards, a second
548 baseline was recorded for 60 s. Association and dissociation of analyte was carried
549 out by dipping the tip first into GST-PirA solution for 180s and then transferring it into
550 buffer solution for further 120s. In every single experiment, one sensor loaded with
551 PII(ΔT) was used as negative control. To investigate the binding of GST tag alone and
552 PirA without the GST-tag to P_{II} protein, parallel experiments were performed in the
553 presence of 2 mM ADP. The interaction curves were achieved by subtracting the
554 control curve and adjusting them to the average of baseline and dissociation steps. In
555 every set of experiment K_D values were calculated by plotting concentration versus
556 maximum response.

557 His_8-tagged variants of P_{II} were prepared as previously described (79). For the
558 preparation of recombinant PirA protein for BLI analysis, the *pirA* gene was cloned into
559 XhoI and EcoRI sites of pGEX-4T-3 vector (GE Healthcare Life Sciences, Freiburg,
560 Germany), encoding recombinant PirA with N-terminal-fused GST-tag. In addition, *pirA*
561 was cloned into SapI-site of pBXC3GH vector (Addgene, Toddington,U.K.), encoding
562 PirA with a C-terminally fused GFP-His_{10}-tag. The plasmids were overexpressed in *E.*
563 *coli* strain BL21(DE3). Purification of PirA with GST or GFP-His_{10} tags was performed
564 as previously described (80, 81). To remove the GFP-His_{10}-tag from PirA, 2.4 mg of
565 recombinant PirA in 750 µl of PirA-buffer (50mM Tris/HCl, 100mM KCl, 100mM NaCl,
566 5mM $MgCl_2$, 0.5mM EDTA, 1mM DTT, pH 7.8) were treated with 50 µl 3C protease

(0.1. mg) at 4˚C over night. Afterwards, 200 µl Ni-NTA agarose beads (QIAGEN GmbH, Hilden, Germany) were added to the mixture and gently shaken at room temperature for 60 min. The beads were removed by filtration and the tag-free PirA protein was dialyzed against PirA buffer containing 50% (v/v) glycerol and stored at -20˚ C until use.

Acknowledgments

The project was funded by grants from the German Research Foundation (DFG) to SK (KL 3114/2-1), KF (Fo195/17-1) and MH (HA 2002/23-1), grants BIO2016-75634-P and PID2019-104513GB-100 from Agencia Estatal de Investigación (AEI) to FJF and MIMP, and BIO-0284 Group from Junta de Andalucía, all co-financed by FEDER (European regional development fund). The LC-MS/MS equipment at University of Rostock was financed through the HBFG program (GZ: INST 264/125-1 FUGG to M.H.). We also acknowledge the use of the facilities of the Centre for Biocatalysis (MiKat) at the Helmholtz Centre for Environmental Research (UFZ). The UFZ is supported by the European Regional Development Funds (EFRE, Europe funds Saxony) and the Helmholtz Association.

References

1. Herrero A, Flores E, Imperial J. 2019. Nitrogen assimilation in bacteria, p. 280–300. *In* Schmidt, TM (ed.), Encyclopedia of Microbiology (Fourth Edition). Academic Press, Oxford.

2. Smercina DN, Evans SE, Friesen ML, Tiemann LK. 2019. To fix or not to fix: Controls on free-living nitrogen fixation in the Rhizosphere. Appl Environ Microbiol 85.

3. Zehr JP, Capone DG. 2020. Changing perspectives in marine nitrogen fixation. Science 368.

4. Magasanik B. 1982. Genetic control of nitrogen assimilation in bacteria. Annu Rev Genet 16:135–168.

6. Reitzer L. 2003. Nitrogen assimilation and global regulation in *Escherichia coli*. Annu Rev Microbiol 57:155–176.

7. van Heeswijk WC, Westerhoff HV, Boogerd FC. 2013. Nitrogen assimilation in *Escherichia coli*: putting molecular data into a systems perspective. Microbiol Mol Biol Rev MMBR 77:628–695.

8. Stadtman ER. 2004. Regulation of glutamine synthetase activity. EcoSal Plus 1.

9. Flombaum P, Gallegos JL, Gordillo RA, Rincón J, Zabala LL, Jiao N, Karl DM, Li WKW, Lomas MW, Veneziano D, Vera CS, Vrugt JA, Martiny AC. 2013. Present and future global distributions of the marine cyanobacteria *Prochlorococcus* and *Synechococcus*. Proc Natl Acad Sci 110:9824–9829.

10. Montoya JP, Holl CM, Zehr JP, Hansen A, Villareal TA, Capone DG. 2004. High rates of N2 fixation by unicellular diazotrophs in the oligotrophic Pacific Ocean. Nature 430:1027–1032.

11. Soo RM, Hemp J, Hugenholtz P. 2019. Evolution of photosynthesis and aerobic respiration in the cyanobacteria. Free Radic Biol Med 140:200–205.

12. Appel J, Hueren V, Boehm M, Gutekunst K. 2020. Cyanobacterial *in vivo* solar hydrogen production using a photosystem I–hydrogenase (PsaD-HoxYH) fusion complex. 6. Nat Energy 5:458–467.

612 13. Ducat DC, Way JC, Silver PA. 2011. Engineering cyanobacteria to generate high-
613 value products. Trends Biotechnol 29:95–103.

614 14. Hagemann M, Hess WR. 2018. Systems and synthetic biology for the
615 biotechnological application of cyanobacteria. Curr Opin Biotechnol 49:94–99.

616 15. Saper G, Kallmann D, Conzuelo F, Zhao F, Tóth TN, Liveanu V, Meir S,
617 Szymanski J, Aharoni A, Schuhmann W, Rothschild A, Schuster G, Adir N. 2018.
618 Live cyanobacteria produce photocurrent and hydrogen using both the respiratory
619 and photosynthetic systems. 1. Nat Commun 9:2168.

620 16. Wijffels RH, Kruse O, Hellingwerf KJ. 2013. Potential of industrial biotechnology
621 with cyanobacteria and eukaryotic microalgae. Curr Opin Biotechnol 24:405–413.

622 17. García-Domínguez M, Reyes JC, Florencio FJ. 1999. Glutamine synthetase
623 inactivation by protein–protein interaction. Proc Natl Acad Sci U S A 96:7161–
624 7166.

625 18. Saelices L, Galmozzi CV, Florencio FJ, Muro-Pastor MI. 2011. Mutational analysis
626 of the inactivating factors, IF7 and IF17 from *Synechocystis* sp. PCC 6803: critical
627 role of arginine amino acid residues for glutamine synthetase inactivation. Mol
628 Microbiol 82:964–975.

629 19. Luque I, Flores E, Herrero A. 1994. Molecular mechanism for the operation of
630 nitrogen control in cyanobacteria. EMBO J 13:2862–2869.

631 20. Giner-Lamia J, Robles-Rengel R, Hernández-Prieto MA, Muro-Pastor MI,
632 Florencio FJ, Futschik ME. 2017. Identification of the direct regulon of NtcA during
633 early acclimation to nitrogen starvation in the cyanobacterium *Synechocystis* sp.
634 PCC 6803. Nucleic Acids Res 45:11800–11820.

635 21. Herrero A, Muro-Pastor AM, Flores E. 2001. Nitrogen control in cyanobacteria. J
636 Bacteriol 183:411–425.

637 22. Herrero A, Muro-Pastor AM, Valladares A, Flores E. 2004. Cellular differentiation
638 and the NtcA transcription factor in filamentous cyanobacteria. FEMS Microbiol
639 Rev 28:469–487.

640 23. Vega-Palas MA, Flores E, Herrero A. 1992. NtcA, a global nitrogen regulator from
641 the cyanobacterium *Synechococcus* that belongs to the Crp family of bacterial
642 regulators. Mol Microbiol 6:1853–1859.

643 24. Espinosa J, Forchhammer K, Burillo S, Contreras A. 2006. Interaction network in
644 cyanobacterial nitrogen regulation: PipX, a protein that interacts in a 2-
645 oxoglutarate dependent manner with P_{II} and NtcA. Mol Microbiol 61:457–469.

646 25. Forcada-Nadal A, Llácer JL, Contreras A, Marco-Marín C, Rubio V. 2018. The P_{II}-
647 NAGK-PipX-NtcA regulatory axis of Cyanobacteria: A tale of changing partners,
648 allosteric effectors and non-covalent interactions. Front Mol Biosci 5.

649 26. Vázquez-Bermúdez MF, Herrero A, Flores E. 2002. 2-Oxoglutarate increases the
650 binding affinity of the NtcA (nitrogen control) transcription factor for the
651 *Synechococcus glnA* promoter. FEBS Lett 512:71–74.

652 27. Forchhammer K, Lüddecke J. 2016. Sensory properties of the P_{II} signalling protein
653 family. FEBS J 283:425–437.

654 28. Forchhammer K, Selim KA. 2020. Carbon/nitrogen homeostasis control in
655 cyanobacteria. FEMS Microbiol Rev 44:33–53.

656 29. Heinrich A, Maheswaran M, Ruppert U, Forchhammer K. 2004. The
657 *Synechococcus elongatus* P_{II} signal transduction protein controls arginine
658 synthesis by complex formation with N-acetyl-l-glutamate kinase. Mol Microbiol
659 52:1303–1314.

660 30. García-Domínguez M, Reyes JC, Florencio FJ. 2000. NtcA represses
661 transcription of *gifA* and *gifB*, genes that encode inhibitors of glutamine synthetase
662 type I from *Synechocystis* sp. PCC 6803. Mol Microbiol 35:1192–1201.

663 31. Bolay P, Muro-Pastor MI, Florencio FJ, Klähn S. 2018. The distinctive regulation
664 of cyanobacterial glutamine synthetase. Life Basel Switz 8.

665 32. Zhang H, Liu Y, Nie X, Liu L, Hua Q, Zhao G-P, Yang C. 2018. The cyanobacterial
666 ornithine–ammonia cycle involves an arginine dihydrolase. Nat Chem Biol 14:575.

667 33. Llácer JL, Espinosa J, Castells MA, Contreras A, Forchhammer K, Rubio V. 2010.
668 Structural basis for the regulation of NtcA-dependent transcription by proteins
669 PipX and P_{II}. Proc Natl Acad Sci U S A 107:15397–15402.

670 34. Galmozzi CV, Fernández-Avila MJ, Reyes JC, Florencio FJ, Muro-Pastor MI.
671 2007. The ammonium-inactivated cyanobacterial glutamine synthetase I is
672 reactivated *in vivo* by a mechanism involving proteolytic removal of its inactivating
673 factors. Mol Microbiol 65:166–179.

674 35. Klähn S, Bolay P, Wright PR, Atilho RM, Brewer KI, Hagemann M, Breaker RR,
675 Hess WR. 2018. A glutamine riboswitch is a key element for the regulation of
676 glutamine synthetase in cyanobacteria. Nucleic Acids Res 46:10082–10094.

677 36. Klähn S, Schaal C, Georg J, Baumgartner D, Knippen G, Hagemann M, Muro-
678 Pastor AM, Hess WR. 2015. The sRNA NsiR4 is involved in nitrogen assimilation

679 control in cyanobacteria by targeting glutamine synthetase inactivating factor IF7.
680 Proc Natl Acad Sci U S A 112:E6243-6252.

681 37. Görl M, Sauer J, Baier T, Forchhammer K. 1998. Nitrogen-starvation-induced
682 chlorosis in *Synechococcus* PCC 7942: adaptation to long-term survival. Microbiol
683 Read Engl 144 (Pt 9):2449–2458.

684 38. Collier JL, Grossman AR. 1994. A small polypeptide triggers complete
685 degradation of light-harvesting phycobiliproteins in nutrient-deprived
686 cyanobacteria. EMBO J 13:1039–1047.

687 39. Llácer JL, Fita I, Rubio V. 2008. Arginine and nitrogen storage. Curr Opin Struct
688 Biol 18:673–681.

689 40. Watzer B, Engelbrecht A, Hauf W, Stahl M, Maldener I, Forchhammer K. 2015.
690 Metabolic pathway engineering using the central signal processor P_{II}. Microb Cell
691 Factories 14:192.

692 41. Watzer B, Spät P, Neumann N, Koch M, Sobotka R, Macek B, Hennrich O,
693 Forchhammer K. 2019. The signal transduction protein P_{II} controls ammonium,
694 nitrate and urea uptake in cyanobacteria. Front Microbiol 10:1428.

695 42. Muro-Pastor MI, Cutillas-Farray Á, Pérez-Rodríguez L, Pérez-Saavedra J, Armas
696 AV, Paredes A, Robles-Rengel R, Florencio FJ. 2020. CfrA, a novel carbon flow
697 regulator, adapts carbon metabolism to nitrogen deficiency in cyanobacteria.
698 Plant Physiol https://doi.org/10.1104/pp.20.00802.

699 43. Orthwein T, Scholl J, Spät P, Lucius S, Koch M, Macek B, Hagemann M,
700 Forchhammer K. 2020. The novel P_{II}-interacting regulator PirC (Sll0944) identifies

3-phosphoglycerate mutase (PGAM) as central control point of carbon storage metabolism in cyanobacteria. bioRxiv 2020.09.11.292599.

44. Forchhammer K. 2008. P(II) signal transducers: novel functional and structural insights. Trends Microbiol 16:65–72.

45. Fokina O, Chellamuthu V-R, Zeth K, Forchhammer K. 2010. A novel signal transduction protein P_{II} variant from *Synechococcus elongatus* PCC 7942 indicates a two-step process for NAGK–P_{II} complex formation. J Mol Biol 399:410–421.

46. Zeth K, Fokina O, Forchhammer K. 2012. An engineered P_{II} protein variant that senses a novel ligand: atomic resolution structure of the complex with citrate. Acta Crystallogr D Biol Crystallogr 68:901–908.

47. Burillo S, Luque I, Fuentes I, Contreras A. 2004. Interactions between the nitrogen signal transduction protein P_{II} and N-acetyl glutamate kinase in organisms that perform oxygenic photosynthesis. J Bacteriol 186:3346–3354.

48. Charlier D, Bervoets I. 2019. Regulation of arginine biosynthesis, catabolism and transport in *Escherichia coli*. Amino Acids 51:1103–1127.

49. Cunin R, Glansdorff N, Piérard A, Stalon V. 1986. Biosynthesis and metabolism of arginine in bacteria. Microbiol Rev 50:314–352.

50. Chellamuthu V-R, Ermilova E, Lapina T, Lüddecke J, Minaeva E, Herrmann C, Hartmann MD, Forchhammer K. 2014. A widespread glutamine-sensing mechanism in the plant kingdom. Cell 159:1188–1199.

722 51. Sugiyama K, Hayakawa T, Kudo T, Ito T, Yamaya T. 2004. Interaction of N-
723 acetylglutamate kinase with a P_{II}-like protein in rice. Plant Cell Physiol 45:1768–
724 1778.

725 52. Li Y, Liu W, Sun L-P, Zhou Z-G. 2017. Evidence for P_{II} with NAGK interaction that
726 regulates Arg synthesis in the microalga *Myrmecia incisa* in response to nitrogen
727 starvation. 1. Sci Rep 7:16291.

728 53. Selim KA, Ermilova E, Forchhammer K. 2020. From cyanobacteria to
729 Archaeplastida: new evolutionary insights into P_{II} signalling in the plant kingdom.
730 New Phytol 227:722–731.

731 54. Leigh JA, Dodsworth JA. 2007. Nitrogen regulation in bacteria and archaea. Annu
732 Rev Microbiol 61:349–377.

733 55. Muro-Pastor MI, Reyes JC, Florencio FJ. 2001. Cyanobacteria perceive nitrogen
734 status by sensing intracellular 2-oxoglutarate levels. J Biol Chem 276:38320–
735 38328.

736 56. Battchikova N, Vainonen JP, Vorontsova N, Keranen M, Carmel D, Aro E-M. 2010.
737 Dynamic changes in the proteome of *Synechocystis* 6803 in response to CO_2)
738 limitation revealed by quantitative proteomics. J Proteome Res 9:5896–5912.

739 57. Orf I, Klähn S, Doreen Schwarz D, Frank M, Hess WR, Hagemann M, Kopka J.
740 2015. Integrated analysis of engineered carbon limitation in a quadruple
741 CO_2/HCO_3^--uptake mutant of *Synechocystis* sp. PCC 6803. Plant Physiol
742 pp.01289.2015.

743 58. Fokina O, Herrmann C, Forchhammer K. 2011. Signal-transduction protein P_{II}
744 from *Synechococcus elongatus* PCC 7942 senses low adenylate energy charge
745 *in vitro*. Biochem J 440:147–156.

746 59. Zeth K, Fokina O, Forchhammer K. 2014. Structural basis and target-specific
747 modulation of ADP sensing by the *Synechococcus elongatus* P_{II} signaling protein.
748 J Biol Chem 289:8960–8972.

749 60. Lüddecke J, Forchhammer K. 2013. From P_{II} signaling to metabolite sensing: a
750 novel 2-oxoglutarate sensor that details P_{II} - NAGK complex formation. PLoS ONE
751 8.

752 61. Sato S, Shimoda Y, Muraki A, Kohara M, Nakamura Y, Tabata S. 2007. A large-
753 scale protein protein interaction analysis in *Synechocystis* sp. PCC6803. DNA
754 Res Int J Rapid Publ Rep Genes Genomes 14:207–216.

755 62. Anfelt J, Hallström B, Nielsen J, Uhlén M, Hudson EP. 2013. Using transcriptomics
756 to improve butanol tolerance of *Synechocystis* sp. strain PCC 6803. Appl Environ
757 Microbiol 79:7419–7427.

758 63. Trinh CT, Huffer S, Clark ME, Blanch HW, Clark DS. 2010. Elucidating
759 mechanisms of solvent toxicity in ethanologenic *Escherichia coli*. Biotechnol
760 Bioeng 106:721–730.

761 64. Volkers RJM, de Jong AL, Hulst AG, van Baar BLM, de Bont JAM, Wery J. 2006.
762 Chemostat-based proteomic analysis of toluene-affected *Pseudomonas putida*
763 S12. Environ Microbiol 8:1674–1679.

764 65. Picossi S, Flores E, Herrero A. 2014. ChIP analysis unravels an exceptionally
765 wide distribution of DNA binding sites for the NtcA transcription factor in a
766 heterocyst-forming cyanobacterium. BMC Genomics 15:22.

767 66. Hanson TE, Forchhammer K, Tandeau de Marsac N, Meeks JC. 1998.
768 Characterization of the *glnB* gene product of *Nostoc punctiforme* strain ATCC
769 29133: *glnB* or the P_{II} protein may be essential. Microbiol Read Engl 144 (Pt
770 6):1537–1547.

771 67. Palinska KA, Laloui W, Bédu S, Loiseaux-de Goer S, Castets AM, Rippka R,
772 Tandeau de Marsac N. 2002. The signal transducer P_{II} and bicarbonate
773 acquisition in *Prochlorococcus marinus* PCC 9511, a marine cyanobacterium
774 naturally deficient in nitrate and nitrite assimilation. Microbiol Read Engl
775 148:2405–2412.

776 68. Flores E, Arévalo S, Burnat M. 2019. Cyanophycin and arginine metabolism in
777 cyanobacteria. Algal Res 42:101577.

778 69. Steglich C, Futschik ME, Lindell D, Voss B, Chisholm SW, Hess WR. 2008. The
779 challenge of regulation in a minimal photoautotroph: Non-coding RNAs in
780 *Prochlorococcus*. PLOS Genet 4:e1000173.

781 70. Rippka R, Deruelles J, Waterbury JB, Herdman M, Stanier RY. 1979. Generic
782 assignments, strain histories and properties of pure cultures of cyanobacteria.
783 Microbiology 111:1–61.

784 71. García-Domínguez M, Lopez-Maury L, Florencio FJ, Reyes JC. 2000. A gene
785 cluster involved in metal homeostasis in the cyanobacterium *Synechocystis* sp.
786 strain PCC 6803. J Bacteriol 182:1507–1514.

787 72. Elhai J, Wolk CP. 1988. A versatile class of positive-selection vectors based on
788 the nonviability of palindrome-containing plasmids that allows cloning into long
789 polylinkers. Gene 68:119–138.

790 73. Pinto FL, Thapper A, Sontheim W, Lindblad P. 2009. Analysis of current and
791 alternative phenol based RNA extraction methodologies for cyanobacteria. BMC
792 Mol Biol 10:79.

793 74. Hein S, Scholz I, Voß B, Hess WR. 2013. Adaptation and modification of three
794 CRISPR loci in two closely related cyanobacteria. RNA Biol 10:852–864.

795 75. Reyes JC, Crespo JL, Garcia-Dominguez M, Florencio FJ. 1995. Electron
796 transport controls glutamine synthetase activity in the facultative heterotrophic
797 cyanobacterium *Synechocystis* sp. PCC 6803. Plant Physiol 109:899–905.

798 76. Laemmli UK. 1970. Cleavage of structural proteins during the assembly of the
799 head of Bacteriophage T4. 5259. Nature 227:680–685.

800 77. Navarro F, Martín-Figueroa E, Florencio FJ. 2000. Electron transport controls
801 transcription of the thioredoxin gene *trxA* in the cyanobacterium *Synechocystis*
802 sp. PCC 6803. Plant Mol Biol 43:23–32.

803 78. Reinholdt O, Schwab S, Zhang Y, Reichheld J-P, Fernie AR, Hagemann M, Timm
804 S. 2019. Redox-regulation of photorespiration through mitochondrial Thioredoxin
805 o1. Plant Physiol 181:442–457.

806 79. Scholl J, Dengler L, Bader L, Forchhammer K. 2020. Phosphoenolpyruvate
807 carboxylase from the cyanobacterium *Synechocystis* sp. PCC 6803 is under
808 global metabolic control by P_{II} signaling. Mol Microbiol 114:292–307.

809 80. Harper S, Speicher DW. 2011. Purification of proteins fused to glutathione S-
810 transferase, p. 259–280. *In* Walls, D, Loughran, ST (eds.), Protein
811 Chromatography: Methods and Protocols. Humana Press, Totowa, NJ.

812 81. Maheswaran M, Urbanke C, Forchhammer K. 2004. Complex Formation and
813 Catalytic Activation by the P_{II} Signaling Protein of *N* -Acetyl-l-glutamate Kinase
814 from *Synechococcus elongatus* Strain PCC 7942. J Biol Chem 279:55202–55210.

815 82. Kumar S, Stecher G, Tamura K. 2016. MEGA7: Molecular evolutionary genetics
816 analysis version 7.0 for bigger datasets. Mol Biol Evol 33:1870–1874.

817 83. Altschul SF, Gish W, Miller W, Myers EW, Lipman DJ. 1990. Basic local alignment
818 search tool. J Mol Biol 215:403–410.

819 84. Mitschke J, Georg J, Scholz I, Sharma CM, Dienst D, Bantscheff J, Voß B,
820 Steglich C, Wilde A, Vogel J, Hess WR. 2011. An experimentally anchored map
821 of transcriptional start sites in the model cyanobacterium *Synechocystis* sp.
822 PCC6803. Proc Natl Acad Sci 108:2124–2129.

823 85. Krasikov V, Aguirre von Wobeser E, Dekker HL, Huisman J, Matthijs HCP. 2012.
824 Time-series resolution of gradual nitrogen starvation and its impact on
825 photosynthesis in the cyanobacterium *Synechocystis* PCC 6803. Physiol Plant
826 145:426–439.

827 86. Schneider CA, Rasband WS, Eliceiri KW. 2012. NIH Image to ImageJ: 25 years
828 of image analysis. Nat Methods 9:671–675.

829

Figures

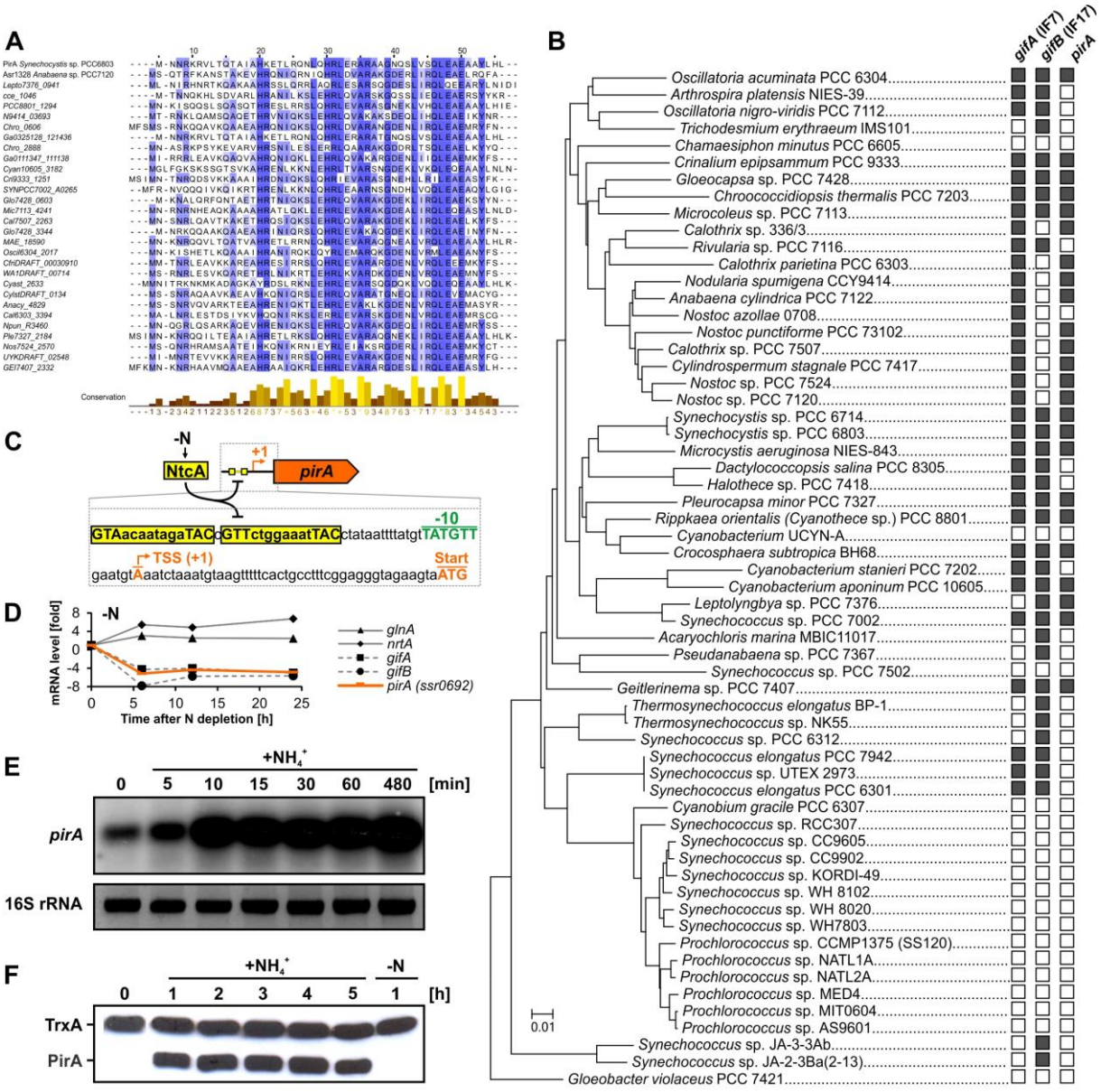

Figure 1: The N-regulated gene *pirA* and its occurrence among cyanobacteria. A: Amino acid alignment of randomly selected cyanobacterial PirA homologs. The alignment was made using ClustalW and visualized by using Jalview. **B:** Phylogenetic tree of selected cyanobacteria based on 16S rDNA sequences. The tree was generated with the MEGA7 (82) software package and the Neighbor-Joining method. Please note that we re-used a calculated tree from our previous publication (35) and assigned the presence of genes in the corresponding genomes manually. Gene presence (illustrated by filled rectangle) was investigated using the BLASTP algorithm (83). As reference the amino acid sequences of PirA, IF7 (GifA, Ssl1911) and IF17 (GifB, Sll1515) from *Synechocystis* were used. **C:** Overview of the promoter region upstream of the *pirA* gene in *Synechocystis*. Two putative NtcA binding sites are highlighted. The transcriptional start site (TSS, +1) and the location of the -10 element were extracted from differential RNAseq data (84). **D:** Changes of mRNA levels for several *Synechocystis* genes in response to N limitation. Data were extracted and plotted from previously published microarray data (85). **E:** Northern blot showing transcript accumulation of *pirA* in nitrate-grown *Synechocystis* cells upon addition of 10 mM ammonium chloride. 16S rRNA was used as loading control **F:** Western blot showing changes in PirA protein levels in response to ammonium upshifts and subsequent N depletion. For this a specific, customized antibody against PirA has been raised in rabbit. An antibody against thioredoxin (TrxA) was used to verify equal loading.

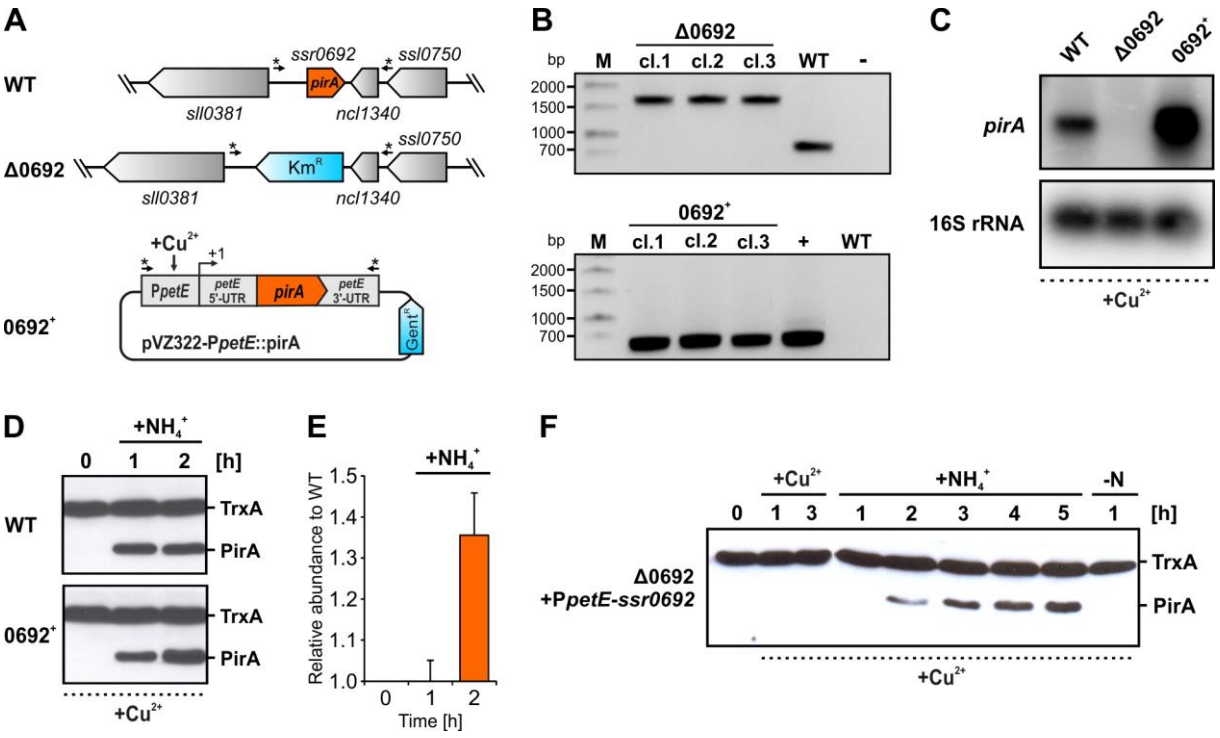

Figure 2: Properties and expression profiles in recombinant strains Δ0692 and 0692$^+$. **A:** Schematic view of the *pirA* locus in the WT and in the knockout strain Δ0692 as well as of a pVZ322 plasmid derivative harboring a *pirA* gene copy under control of the Cu^{2+}-inducible promoter P*petE* that is present in the overexpression strain 0692$^+$. In the Δ0692 knockout strain, *pirA* was replaced by a kanamycin resistance cassette (Km^R) via homologous recombination. The plasmid enabling ectopic *pirA* expression was introduced into *Synechocystis* WT. The arrows labelled with asterisks indicate the binding sites for primers used to verify the mutants. **B:** PCR verification of the genotype of independently obtained mutant strains. In each case three clones were tested using primer combinations Ssr0692_KO-seg_fw/Ssr0692_KO-seg_rev (in case of Δ0692) or PpetE_fw(XhoI) and Toop_rev(AseI) (in case of 0692$^+$). M, marker; bp, base pairs; cl., clone; –, negative control (water as template); +, positive control (purified plasmid as template). **C:** Relative abundance of the *pirA* mRNA, measured via northern blot using sequence specific ^{32}P-labelled ssRNA probes. In all cases RNA was isolated from cells grown in presence of 1µM $CuSO_4$. **D:** Western blot showing PirA protein levels in cells of the WT and strain 0692$^+$, treated with 1 µM Cu^{2+} for 3 hours and afterwards with 10 mM ammonium. Thioredoxin (TrxA) levels verify equal loading. **E:** PirA levels relative to WT. Data were obtained by densitometric evaluation of respective bands using the ImageJ software (86). Data are the mean ± SD of values obtained from two independent western blots, i.e. two biological replicates (independent clones). **F:** PirA accumulation in a Δ0692 strain that was complemented with a *pirA* gene fused to the *petE* promoter. Please note that the data shown here were obtained using a mutant in which the P*petE*-*pirA* construct was integrated into the chromosome, i.e. this strain does not harbor the plasmid derivative shown in panel A.

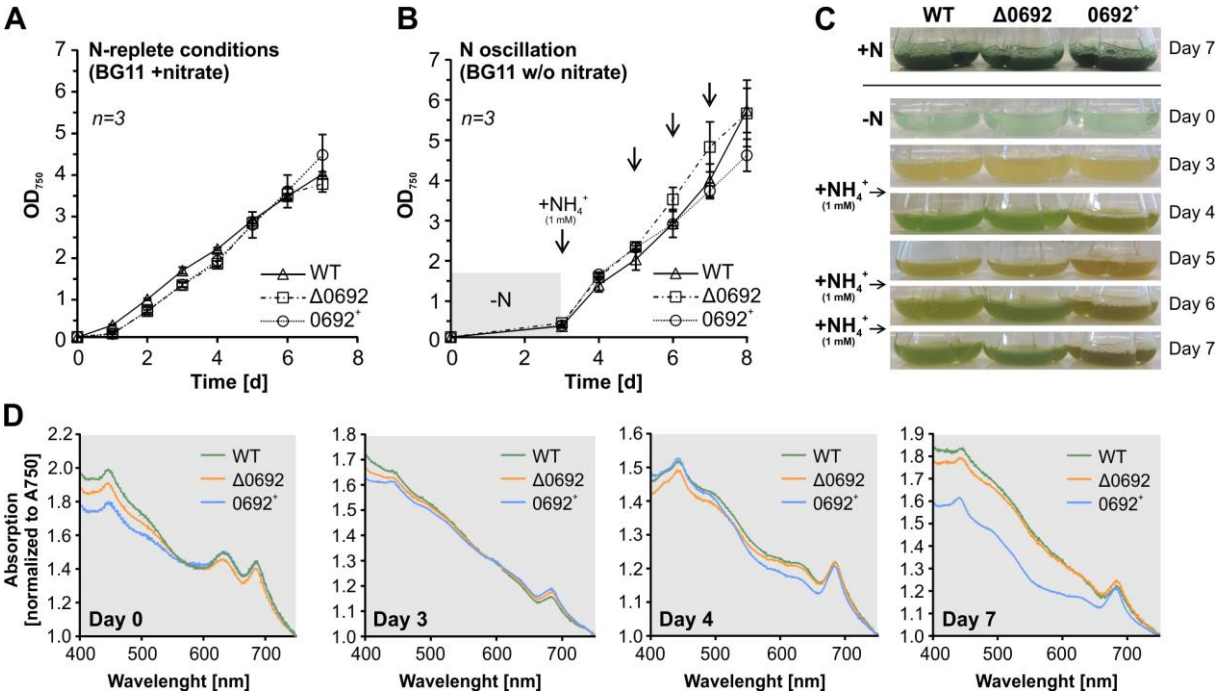

868

869 **Figure 3: Growth and pigmentation of the WT and the mutant strains Δ0692 and 0692+ when N is oscillating**.
870 **A, B:** Growth under standard conditions and when ammonium is consecutively added to N starved cultures. Arrows
871 indicate time points at which 1 mM NH_4Cl was added. Data are the mean ± SD of three independent cultures
872 (including three independent clones of each mutant). **C:** Representative photographs of cultures used in the
873 experiment. Ammonium was added after day 3 and repeated after days 5 and 6. **D:** Whole cell absorption spectra.
874 Values were normalized to A_{750} values.

875

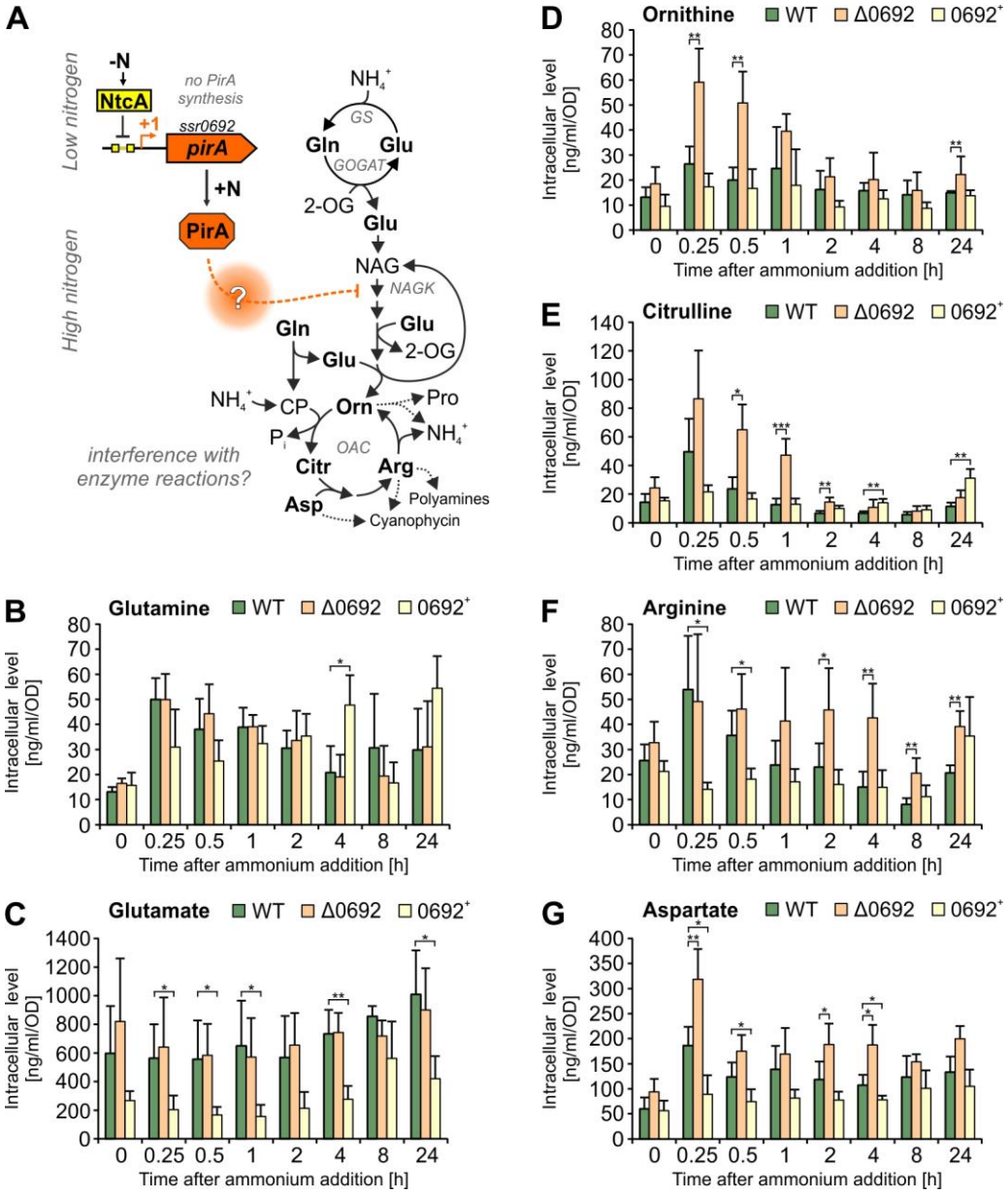

876

877 **Figure 4: Kinetics of metabolites linked to the OAC cycle in response to ammonium addition. A:** Simplified
878 overview of metabolic pathways associated with ammonium assimilation and a possible regulatory impact of PirA
879 on certain enzymatic reactions. 2-OG - 2-oxoglutarate, CP - carbamoyl phosphate, GS - glutamine synthetase,
880 GOGAT - glutamine oxoglutarate aminotransferase, NAG - N-acetyl-glutamate, NAGK - N-acetyl glutamate kinase,
881 OAC - ornithine-ammonia cycle. **B-G:** Kinetics of selected metabolites after adding 10 mM ammonium to nitrate-
882 grown cells in the exponential phase. Metabolites were determined by UHPLC-MS/MS after ethanol extraction from
883 cells of the WT, Δ0692 and 0692$^+$. Data are the mean ± SD of two independent experiments, each conducted with
884 three biological replicates (independent clones). Significant differences between the strains are labeled and were
885 revealed by one-way analysis of variance (ANOVA; * $p<0.05$, ** $p<0.01$, *** $p<0.001$).

886

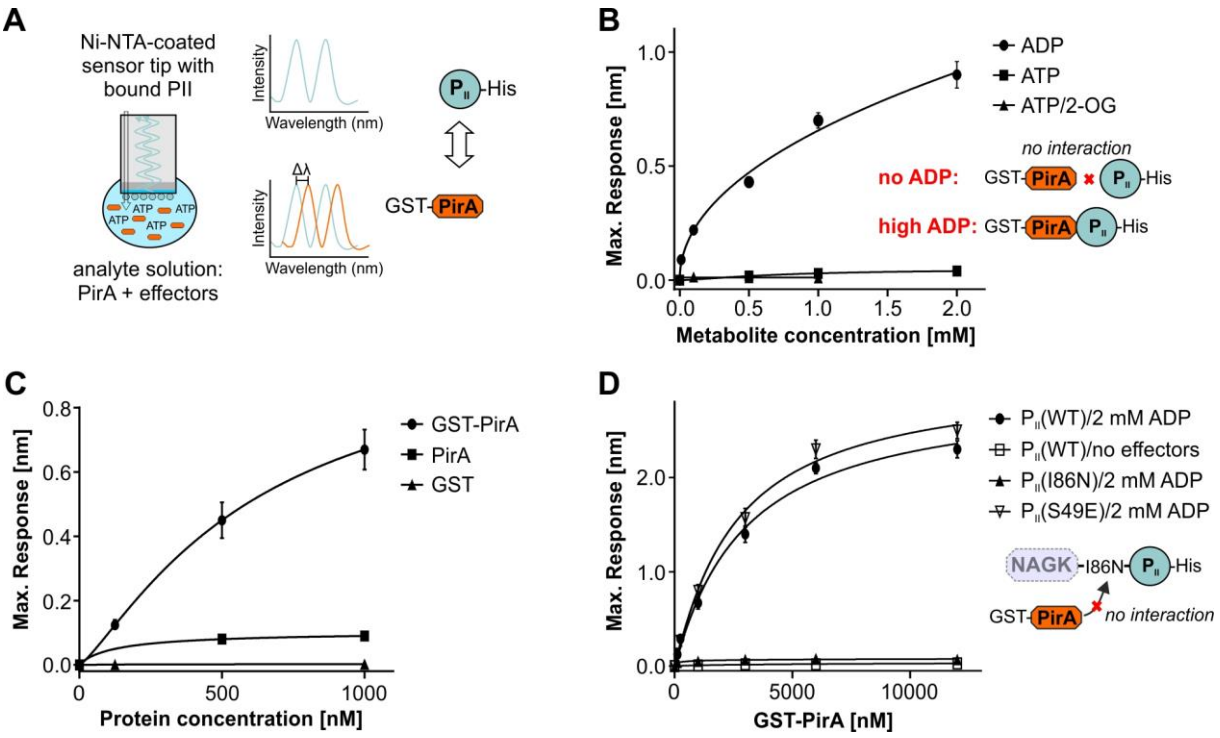

Figure 5: Determination of complex formation between PirA the P_{II} protein measured by Bio-layer interferometry (BLI). A: Schematic view of the measuring principle. **B:** Representation of the maximum binding response of P_{II}(WT)-His and GST-PirA interaction in the presence of different concentrations of ADP, ATP or ATP/2-OG. **C:** The maximum binding response at different protein concentrations of GST-PirA, tag-free PirA or free GST in the presence of 2 mM ADP. As the binding response is a function of the mass of bound interactor, the response with GST-tagged PirA is correspondingly higher than with isolated PirA peptide. **D:** Representation of the maximum binding response at increasing concentrations of GST-PirA in the absence of effector molecules or in the presence of 2 mM ADP with three different T-loop variants of P_{II}. Data are the mean ± SD of triplicate measurements.

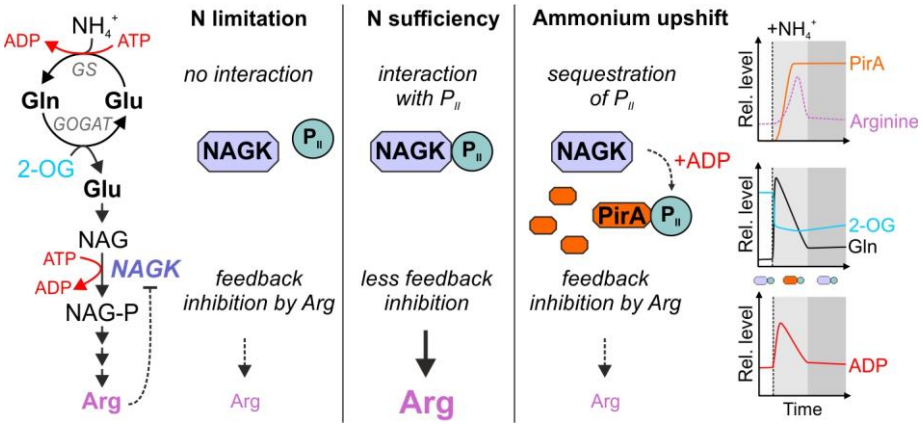

Figure 6: Anticipated model of PirA function. Metabolite kinetics have been approximated based on available literature data (32, 35). Upon shifts in the ammonium concentration PirA accumulates via 2-OG dependent de-repression of the *pirA* gene. The gene product is presumably required to slow down ATP-consuming synthesis of arginine. This could be achieved by ADP-dependent sequestration of P_{II} protein bound to NAGK which is required to diminish feedback inhibition of the enzyme and in turn activate arginine synthesis. The sequestration of P_{II} results in stronger arginine feedback inhibition of NAGK diminishing energy consumption and flux into arginine. After metabolic reorganization (e.g. by inactivating glutamine synthetase activity and decreasing ATP consumption), ADP levels may fall below a critical level preventing interaction between PirA and P_{II}. Accordingly, a higher fraction of the P_{II} pool will again interact with and activate NAGK, which in turn results in elevated arginine synthesis.

Appendix

Supplementary Table S1: Primers used in this study.

Designation	5‘-3‘ sequence	Used for
5’petE-ssr0692_rev	gattattcatacttcttggcgattgtatct	Amplification of *petE* 5’UTR
PpetE_fw(XhoI)	actcgaggaagggatagcaagc	Amplification of *petE* 5’UTR
3’petE-ssr0692_fw	cacctgtaatcagccagctcaatct	Amplification of *petE* 3’UTR
Toop_rev(AseI)	gattaataataaaaaacgcccggcgg	Amplification of *petE* 3’UTR
ssr0692_fw	ccaagaagtatgaataatcgtaaacgtgttttga	Amplification of *ssr0692*
ssr0692_rev	gctggctgattacaggtggagataagca	Amplification of *ssr0692*
Ssr0692-Probe_T7_fw	taatacgactcactatagggctaaggactgattgccggcg	Probe template generation for northern blot specific for *ssr0692*
Ssr0692-Probe_rev	gaataatcgtaaacgtgttttgactcaaac	Probe template generation for northern blot specific for *ssr0692*
Ssr0692upst_fw	tcagcaagatagagtttccacttcggt	Amplification of *ssr0692* upstream region
Ssr0692upst_rev	cggccgcgtttccacaagaataagctcaa	Amplification of *ssr0692* upstream region
KmR_fw	ttgtggaaacgcggccgcag	Amplification of Kanamycin resistance casette
KmR_rev	acaatagataaataaaaaacgcccggc	Amplification of Kanamycin resistance casette
Ssr0692dwnst_fw	gttttttatttatctattgttactgaagttaacaaaaatgt	Amplification of *ssr0692* downstream region
Ssr0692dwnst_rev	ctagaaagattctgggggggaagg	Amplification of *ssr0692* downstream region
Ssr0692_KO-seg_fw	tcagaccgaagtggaaact	Segregation primer for *ssr0692* knockout verification
Ssr0692_KO-seg_rev	gtacttttcaagcggcca	Segregation primer for *ssr0692* knockout verification
5sRNA_for	taatacgactcactataggagaaagaggaacttggcatcggac	Probe template generation for northern blot specific for 5s rRNA
5sRNA_rev	gtcatggaaccactccgatccc	Probe template generation for northern blot specific for 5s rRNA
Ssr0692ORF-fw	gctactaatgaataatcgtaaacgtg	Amplification of *ssr0692*

Ssr0692ORF-rv	gctactcgaggtggagataagcagcttc	Amplification of *ssr0692*
ssr0692.KpnI	gctggtaccatgaataatcgtaaacgtg	Amplification of *ssr0692*
ssr0692.HisBamHI	gctggatccttagtggtggtggtggtggtgcaggtgga gataagcagc	Amplification of *ssr0692*
P*petE*.KpnI.1	gctggtaccctcagggagcgacttcagc	Amplification of P*petE*
P*petE*.KpnI.2.	gctggtaccacttcttggcgattgtatc	Amplification of P*petE*

913

914

915

916 **Supplementary Table S2: Strains used in this study.**

Strain name	Source	Parental strain	Features
WT	Norio Murata (Jap.)	-	*Synechocystis* sp. PCC 6803, wild type, glucose-tolerant, non-motile
Δ0692	This study	*Synechocystis* sp. PCC 6803 wild type	recombinant *Synechocystis* strain in which the *pirA* gene was deleted and replaced by a kanamycin resistance cassette
0692^{+}	This study	*Synechocystis* sp. PCC 6803 wild type	recombinant *Synechocystis* strain carrying the pVZ322-PpetE:*ssr0692* plasmid used for ectopic, Cu^{2+}-inducible *pirA* expression
Δ0692 + PpetE-ssr0692	This study	Δ0692	knockout strain for *pirA* with a PpetE::*ssr0692* construct inserted into the chromosome

917

918

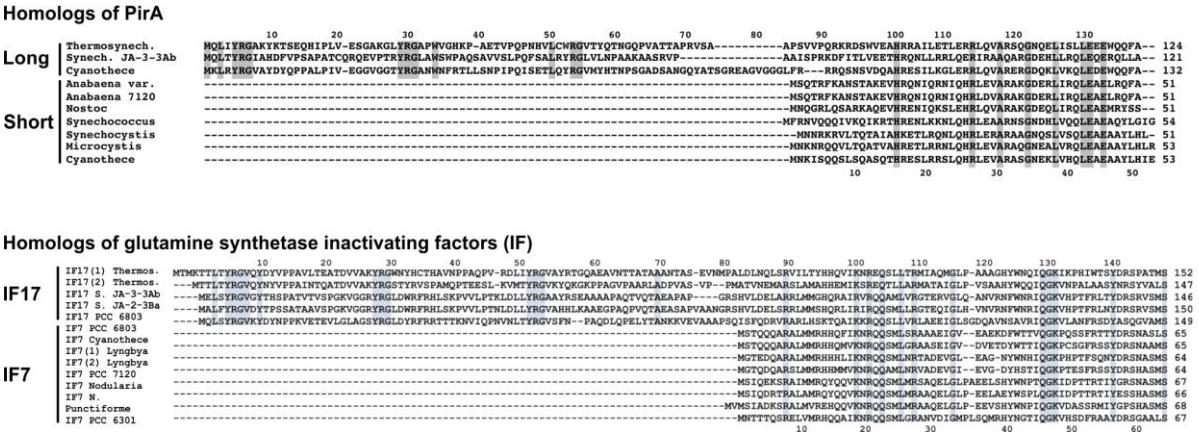

Supplementary Figure S1: Alternative PirA variants. BLASTP analyses suggest alternative PirA versions with an extended N-terminal end in few strains. This resembles the glutamine synthetase (GS) inactivating factors (IF) all of which show a homologous C-terminus but only some show an N-terminal extension. These extensions show conserved amino acid residues that confer stability to the proteins that carry it (18). Those residues are also present in the N-terminal part of alternative PirA versions.